Origin of light-induced states in intense laser fields and their observability in photoelectron spectra

Tomokazu Yasuike and Kiyohiko Someda*

Department of Basic Science, Graduate School of Arts and Sciences, University of Tokyo, Komaba, Meguro-ku, Tokyo 153-8902, Japan

On the basis of the complex-scaled Floquet formalism, metastable states in intense laser fields are investigated by tracing the motion of resonance poles on the complex-energy Riemann surface. We analyzed a model system, in which an electron trapped in a one-dimensional potential well is exposed to an intense laser field. The formation of light-induced states (LIS) is found to be ubiquitous for a wide range of laser frequency. The mathematical origin of LIS, however, depends on the laser frequency. When the laser frequency is tuned to or lower than the one-photon ionization threshold, the LIS originates from a shadow pole of the original bound state. In such a case, the LIS's are predicted to be experimentally detectable as intense peaks in photoelectron spectrum.

I. INTRODUCTION

In the last decade, the science of intense laser fields [1,2] has led to many discoveries of various phenomena originating from nonperturbative interaction between molecules and photon fields. For instance, formation of dressed states [3,4], above-threshold dissociation [3], above-threshold ionization [1,5], tunnel ionization [1,6], and Coulomb explosion [7,8] have intensively been investigated by many experimentalists and theoreticians. Intense laser fields open a doorway to the quantum control exempted from restrictions originating from intrinsic characters of atomic and molecular electronic states. Recently, a symbolic experiment has been reported [9]: The closed-loop optimal control technique combined with intense fields has successfully realized bond-selective molecular dissociation and rearrangement. This has proven that the use of intense laser gains the advantage over the conventional photochemical method.

Recently, experimental preparation of an intense laser pulse has been routinely done particularly in the domain of low frequency ranging from 10^{14} to 10^{15} s^{-1}, and a considerable number of experiments have been reported. From the theoretical point of view, atomic and molecular behavior in the low-frequency domain can be understood on the basis of electronic states in a static field and their adiabatic changes in accordance with the oscillation of field [10].

On the other hand, experimental studies in the domain of high frequency are lacking due to experimental difficulties. From the theoretical point of view, high-frequency intense fields can be treated by the Kramers-Henneberger approximation [11–13], and several theoretical works have predicted intriguing phenomena, such as stabilization [14–16], radiative distortion of atomic [17–19] and molecular [20,21] wave functions, and alignment of molecules [20,22]. The Kramers-Henneberger approximation is based on the following physical picture: Intense laser fields modify the potential-energy function that governs the electron motion in atoms and molecules. The modified potential-energy function could give rise to extra electronic states. Such a possibility has

been discussed by several authors [16,23–26]. The electronic states thus formed in the presence of light field are called light-induced states (LIS's). The character of LIS's would differ from that of atomic and molecular eigenstates, and in the nature of things, it depends sensitively on the intensity and frequency of laser fields. The use of LIS's could open unexplored aspects of quantum control.

No experimental observation of LIS's has been reported so far. Further theoretical study is needed in order to answer the question: Whether LIS's are experimentally detectable in the realistic condition or not? In the present study, we discuss the origin, character, and detectability of LIS's by analyzing electron scattering in intense fields.

Under laser fields of a finite intensity, all the atomic and molecular bound states are subject to photoionization and inevitably become metastable states. They are resonances from the scattering theoretical point of view [27], and are identified as poles of resolvent, $G(E)=(E-H)^{-1}$, in the appropriate domain of complex-energy Riemann surface called a "resonance sector." In general, the resolvent has poles outside the resonance sector. Such poles have no physical meaning, and we hereafter call them "ghost pole."

By changing the laser intensity, the poles move about on the Riemann surface. Therefore, a ghost pole would become a resonance pole, and vice versa. This indicates the birth and death of metastable electronic states. An LIS is identified as the pole that enters the resonance sector when one increases the laser intensity. By tracing the precursor ghost pole in the limit of null field, one can discuss the origin of LIS's. In fact, Fearnside, Potvliege, and Shakeshaft have analyzed a one-dimensional model mimicking the Cl$^-$ ion under irradiation of ArF laser [28], and have shown that the LIS pole correlates with a virtual pole [27], which is a kind of ghost pole, in the limit of null field.

We numerically solve the time-dependent Schrödinger equation based on the complex-scaled Floquet formalism. Therefore, we are able to calculate the pole positions for a wide range of laser frequency and intensity, and grasp systematic behavior of metastable states in intense laser fields.

In the present paper, we analyze a model system mimicking an atom in an intense field: An electron trapped in a one-dimensional potential well is exposed to an intense laser

---

*Author to whom correspondence should be addressed.

field. Although the model is very simple, several nontrivial phenomena are seen including the formation of LIS's. By increasing laser intensity with fixed frequency, the trajectories of poles on the complex-energy Riemann surface are obtained, and the behavior of LIS's is analyzed. We studied the case wherein the laser frequency is equal to or lower than the one-photon ionization threshold, i.e., $\omega \leq E_0/\hbar$, where E_0 is the binding energy of the original bound state in the null field. The LIS is found to originate from a shadow pole of the original bound state. We calculated photoelectron spectra, and found that LIS's are most clearly be observed when one uses the laser with $\omega \sim E_0/\hbar$.

II. MODEL AND BASIC CONCEPTS

A. Model system

We analyze a simple model mimicking an atom: An electron is trapped in a one-dimensional potential well,

$$U(x) = -\frac{1}{\cosh^2 x}, \qquad (1)$$

which gives rise to only one bound state at $E = -\frac{1}{2}$. As will be discussed later, it is important to choose an appropriate gauge for describing systems in intense laser fields. In the momentum representation, one can easily carry out gauge transformations. We, therefore, employ the momentum representation. The potential function, Eq. (1), in the momentum representation has a simple analytic form,

$$\langle p|U|p'\rangle = U(p'-p) = -\frac{p'-p}{2\sinh\left\{\frac{\pi}{2}(p'-p)\right\}}. \qquad (2)$$

In the presence of laser field, the system is described by the time-dependent Schrödinger equation,

$$i\frac{\partial}{\partial t}\Psi(p,t) = H(p,t)\Psi(p,t) = \frac{1}{2}\left(p + \frac{1}{c}A(t)\right)^2 \Psi(p,t)$$
$$+ \int_{-\infty}^{+\infty} dp'\, U(p'-p)\Psi(p',t), \qquad (3)$$

where the vector potential $A(t)$ is given by

$$A(t) = \frac{cF}{\omega}\cos \omega t, \qquad (4)$$

p denotes the momentum, F is the strength of electric field, ω is the laser frequency, and c is the light velocity. The atomic units are employed. The dipole approximation is adopted, i.e., x dependence of the vector potential $A(t)$ is ignored.

B. Floquet formalism

According to the Floquet theorem [29,30], the solutions of time-periodic Schrödinger equation, Eq. (3), can be represented as the quasienergy state (QES) of the form

$$\Psi(p,t) = e^{-iEt}\Phi(p,t), \qquad (5)$$

where $\Phi(t + 2\pi/\omega) = \Phi(t)$. From Eqs. (3) and (5), one can derive the equation

$$\left(H(p,t) - i\frac{\partial}{\partial t}\right)\Phi(p,t) = E\Phi(p,t). \qquad (6)$$

This equation indicates that the function $\Phi(x,t)$ is an eigenfunction of the Floquet Hamiltonian

$$H_F \equiv H(p,t) - i\frac{\partial}{\partial t}. \qquad (7)$$

Since the Floquet eigenfunction $\Phi(p,t)$ is time periodic, it can be expanded in the Fourier series. By introducing the inner product

$$\langle f|g\rangle_t = \frac{\omega}{2\pi}\int_0^{2\pi/\omega} f^*(t')g(t')dt', \qquad (8)$$

the Fourier series expansion can be interpreted as the basis-set expansion with the basis set $\{e^{in\omega t}\}$, and can be expressed in Dirac's notation as

$$\Phi(p,t) = \sum_{n=-\infty}^{\infty} |n\rangle\langle n|\Phi\rangle_t = \sum_{n=-\infty}^{\infty} \Phi_n(p)|n\rangle, \qquad (9)$$

where $\Phi_n(p) \equiv \langle n|\Phi\rangle_t$ and $|n\rangle \equiv e^{in\omega t}$. The Floquet eigenfunction $\Phi(p,t)$ is regarded as a stationary vector in the extended Hilbert space equipped with the generalized inner product,

$$\langle\langle f|g\rangle\rangle = \frac{\omega}{2\pi}\int_0^{2\pi/\omega} dt'\int_{-\infty}^{+\infty} dp\, f^*(p,t')g(p,t'). \qquad (10)$$

The set of Floquet eigenfunctions entirely spans the extended Hilbert space [30]. On the basis of this framework, one can formulate a time-independent scattering theory for time-periodic systems [36]. We adopt such a formalism for simulating photoelectron spectra in intense laser fields in Sec. V.

By substituting Eq. (9) into Eq. (6), one obtains the Floquet-coupled equation

$$\{H_0 + n\omega - E\}\Phi_n(p) - \sum_m H_{m-n}\Phi_m(p) = 0, \qquad (11)$$

where

$$H_\mu = \frac{\omega}{2\pi}\int_0^{2\pi/\omega} H(t')e^{i\mu\omega t'}dt'.$$

One can thus convert a time-periodic system, Eq. (3), into a multichannel stationary problem, Eq. (11), by virtue of the Floquet theory.

Although the laser fields are treated as classical electromagnetic fields in the above formalism, one can use the notion of photons on appropriate occasions. Each Fourier component in Eq. (9) can be interpreted as the photon-number

state [29]. Usually, the QES is a superposition of many different photon-number states and is called the "dressed" state.

C. Multichannel resonance and Riemann sheets

From the scattering theoretical point of view, atomic and molecular eigenstates are defined as the poles of resolvent, $G(E)=(E-H_F)^{-1}$. The resolvent has branch points at every channel thresholds, and one needs to consider Riemann sheets. As mentioned briefly in Sec. I, the physical meaning of the pole depends on the sheet which it inhabits.

In single-channel problems, the complex-energy Riemann surface is composed of two sheets. Each sheet is specified by the sign of the imaginary part of momentum p. For N-channel problems, one needs to specify the sign of each channel momentum p_n, and the Riemann surface is composed of 2^N sheets. Each sheet is identified by the set of signatures $\Sigma=(\sigma_1,\sigma_2,\ldots,\sigma_N)$, where σ_n denotes the sign of Im p_n.

In the asymptotic region $x\to\pm\infty$, the multichannel wave function of resonance satisfies the Siegert boundary condition, i.e., it should behave as outgoing wave in the open channels and should vanish in the closed channels. It follows that the multichannel resonance pole should be on the sheet specified as Σ with $\sigma_{\text{open}}=-$ and $\sigma_{\text{closed}}=+$. Such a sheet is called the resonance sector.

In multichannel problems, each bound state or resonance pole is accompanied by a series of shadow poles [31]. Suppose that there is a bound-state pole on the physical sheet in the uncoupled system. When the coupling is switched on, poles arise on the other sheets at almost the same complex energy. These poles are called "shadow" poles. The shadow pole is a kind of ghost pole, and a cogent candidate for the origin of LIS's [32].

D. Method of numerical calculation

The pole positions were numerically obtained in accordance with the complex-scaling Fourier-grid Hamiltonian (CSFGH) method by Yao and Chu [16]. The only difference between their method and ours is in the choice of gauge. Yao and Chu carried out their calculation in the acceleration gauge, but we employed the velocity gauge. In the velocity gauge, the Floquet-coupled equation, Eq. (11), contains vanishing H_n ($|n|\geqslant 2$), while all the H_n's are nonvanishing in the acceleration gauge. This difference affects the conver-

gence of calculation. By using the momentum representation, the gauge transformation can easily be carried out as the need arises.

We briefly describe the CSFGH procedure in the present study. In the velocity gauge, the Floquet-coupled equation, Eq. (11), is expressed as

$$\{H_0+n\omega-E\}\Phi_n(p)-H_1\Phi_{n+1}(p)-H_{-1}\Phi_{n-1}(p)=0, \tag{12}$$

where

$$H_0=\frac{p^2}{2}+\int_{-\infty}^{\infty}dp\int_{-\infty}^{\infty}dp'|p\rangle\langle p|U|p'\rangle\langle p'|, \tag{13}$$

and

$$H_{+1}=H_{-1}=\frac{pF}{2\omega}. \tag{14}$$

In order to find the QES satisfying the Siegert boundary condition, the Floquet-coupled equation was transformed by the complex scaling in the momentum space $p\to pe^{-i\theta}$ [33]. The momentum p was discretized as

$$p_\mu=\mu\Delta p \quad (\mu=-m,-m+1,\ldots,0,\ldots,m-1,m). \tag{15}$$

The total number of grid points is $N_p=2m+1$. The resultant matrix representations of the operators $H_{0,\pm 1}$ are given by

$$\langle p_\mu|H_0|p_\nu\rangle=\frac{p_\mu^2}{2}e^{-2i\theta}\delta_{\mu,\nu}$$
$$-\frac{(p_\nu-p_\mu)e^{-i\theta}}{2\sinh\left\{\frac{\pi}{2}(p_\nu-p_\mu)e^{-i\theta}\right\}}\Delta pe^{-i\theta} \tag{16}$$

and

$$\langle p_\mu|H_{\pm 1}|p_\nu\rangle=\frac{p_\mu F}{2\omega}e^{-i\theta}\delta_{\mu,\nu}. \tag{17}$$

In this manner, the Floquet-coupled equation is converted into the eigenvalue problem of the Floquet Hamiltonian matrix,

$$\mathbf{H}_F\equiv\begin{pmatrix}\ddots & & & & & \\ & \mathbf{H}_0+2\hbar\omega\mathbf{I} & \mathbf{H}_{+1} & \mathbf{0} & & \\ & \mathbf{H}_{-1} & \mathbf{H}_0+\hbar\omega\mathbf{I} & \mathbf{H}_{+1} & \mathbf{0} & \\ & \mathbf{0} & \mathbf{H}_{-1} & \mathbf{H}_0 & \mathbf{H}_{+1} & \mathbf{0} \\ & & \mathbf{0} & \mathbf{H}_{-1} & \mathbf{H}_0-\hbar\omega\mathbf{I} & \mathbf{H}_{+1} \\ & & & \mathbf{0} & \mathbf{H}_{-1} & \mathbf{H}_0-2\hbar\omega\mathbf{I} \\ & & & & & \ddots\end{pmatrix}, \tag{18}$$

where $\mathbf{I}$ is the $N_p \times N_p$ unit matrix. Due to the above complex-scaling transformation, the Floquet Hamiltonian matrix $\mathbf{H}_F$ is complex symmetric, and gives complex eigenvalues. We solved the eigenvalue problem of $\mathbf{H}_F$. The complex eigenvalues give the pole positions, and the eigenvectors correspond to the resonance wave functions.

In the calculation of pole trajectories described in Sec. III, the spacing of grid, Δp, was chosen to be 0.15, the total number of grid points, N_p, was 101, and the total number of Floquet blocks, N_F, was 21. These parameters led to sufficient convergence of the complex eigenvalues within the relative uncertainty of 10^{-4}. The position of the pole was determined by the variational principle with respect to the parameter of complex scaling, θ [33]. In the simulation of photoelectron spectra described in Sec. V, more fine spacing ($\Delta p = 0.05$) and more grid points ($N_p = 301$) were used.

III. TRAJECTORIES OF POLES AND THE ORIGIN OF LIGHT-INDUCED STATES

A. Trajectories of poles on the complex-energy Riemann surface

Positions of poles on the complex-energy plane are determined by the CSFGH calculation with many different laser intensities and fixed frequency. Trajectories are drawn by connecting these pole positions. They indicate the adiabatic changes of each resonance state when the laser intensity is changed at an infinitely slow rate. In Figs. 1–3, the trajectories for six different laser frequencies are shown.

In these figures, the symbol T_n indicates the threshold of the nth Floquet channel, $E = n\hbar\omega$. We specify each trajectory by using the symbol $\Phi_N^{(\sigma_{-3}, \sigma_{-2}, \sigma_{-1})}$. The superscript indicates the sheet on which the pole exists. The three signatures σ_{-3}, σ_{-2}, σ_{-1} are sufficient to specify the resonance sector in the region of $T_{-3} \lesssim \text{Re}(E) \lesssim T_0$. The subscript N indicates that the pole trajectory comes to the point $E = E_0 + N\hbar\omega$ on the real axis in the limit of null field. For instance, the pole denoted by Φ_0^Σ comes to $E = E_0$, i.e., correlates with the bound state at $E = E_0$ in the limit of null field. The numbers written along trajectory are the values of the ponderomotive radius $\alpha = F/\omega^2$, which is the amplitude of classical quiver motion of electrons driven by laser fields [12]. Since each pole trajectory has as a fixed value of frequency ω, the value of α is useful to indicate the laser intensity.

Due to the time periodicity of the Hamiltonian, the energy spectrum has a translational symmetry with the period of $\hbar\omega$ in the direction of real axis. In Figs. 1–3 we display only Φ_0^Σ, and the other trajectories are omitted for the sake of simplicity. For instance, the trajectory of $\Phi_{+1}^{(---)}$, existing in the region of $T_{-1} < \text{Re}(E) < T_0$, is not displayed in Fig. 1.

B. Origin of a LIS and its shift with changing laser frequency

The trajectories in the case of $\hbar\omega = 0.55$ are shown in Fig. 1(a). The resonance state $\Phi_0^{(---)}$ correlates with the original bound state in the limit of null field. Thus the trajectory of $\Phi_0^{(---)}$ represents the adiabatic change of the original bound state. In the vicinity of $\alpha = 0$, the lifetime of resonance
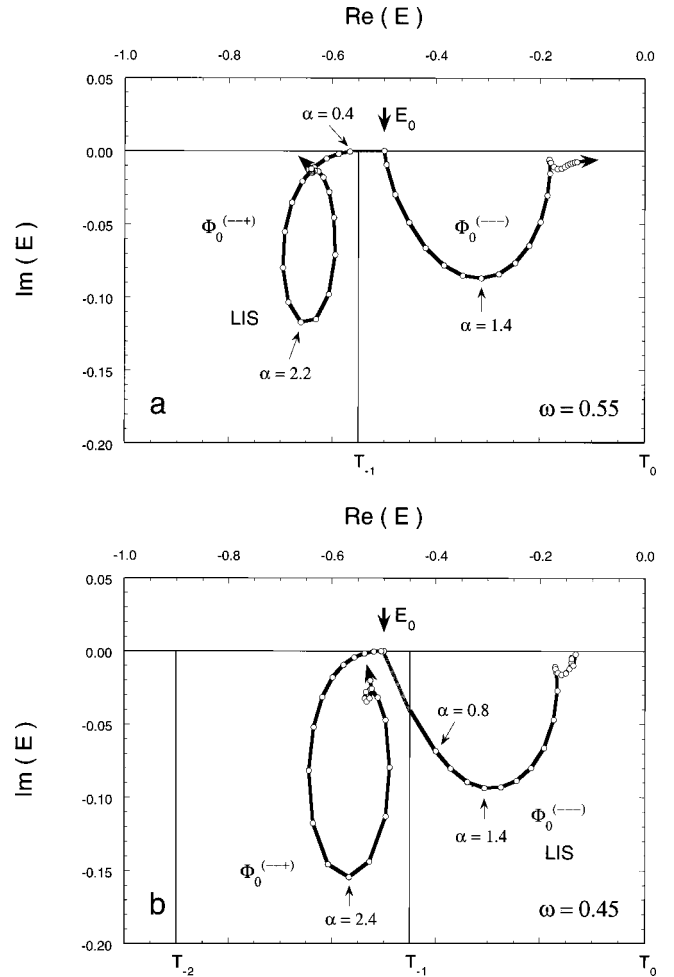

FIG. 1. Pole trajectories on the complex-energy plane with changing α from 0.0 to 5.0. T_N denotes the N-photon threshold, $\text{Re}(E) = N\hbar\omega$. (a) The case of $\omega = 0.55$, and (b) $\omega = 0.45$.

state $\Phi_0^{(---)}$ decreases with increasing α. When the laser intensity exceeds the critical value $\alpha \sim 1.4$, the pole trajectory goes upwards, i.e., the lifetime increases with increasing α. Such a phenomenon is known as stabilization [14–16].

On the other hand, the resonance state $\Phi_0^{(--+)}$ appears on the resonance sector at $\alpha = 0.4$. It lies outside the resonance sector when $0 \leq \alpha < 0.4$, and can be identified as a LIS. This LIS also exhibits stabilization when $\alpha > 2.2$. When $\alpha < 0.4$, the LIS pole becomes a ghost pole, and seems to merge with the pole of the original bound state at $E = -0.5$. This implies that the LIS pole $\Phi_0^{(--+)}$ originates from a shadow pole of the original bound state. Such merger of pole trajectories of $\Phi_0^{(---)}$ and $\Phi_0^{(--+)}$ is also found in the case of $\hbar\omega = 0.45$.

The case of $\hbar\omega = 0.45$ is displayed in Fig. 1(b). One finds the pole trajectories similar to the case of $\hbar\omega = 0.55$. The merger of two trajectories at $E = -0.5$ is again seen. In this case, however, the state staying in the resonance sector in the limit of $\alpha \to 0$ is not $\Phi_0^{(---)}$ but $\Phi_0^{(--+)}$. Namely, $\Phi_0^{(--+)}$ represents the resonance state adiabatically grown from the original bound state, while $\Phi_0^{(---)}$ is identified as a LIS.
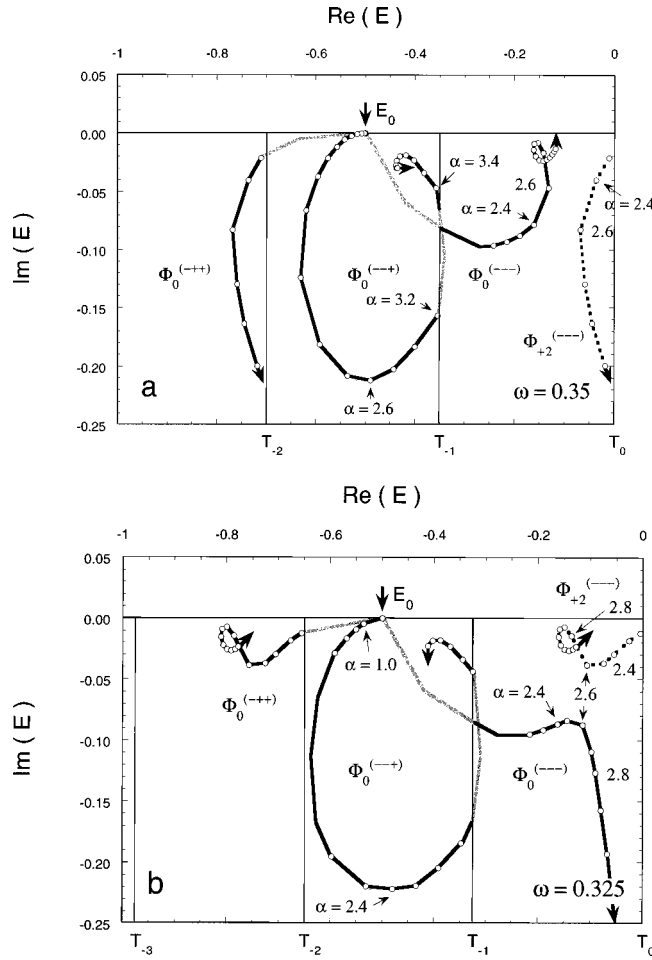
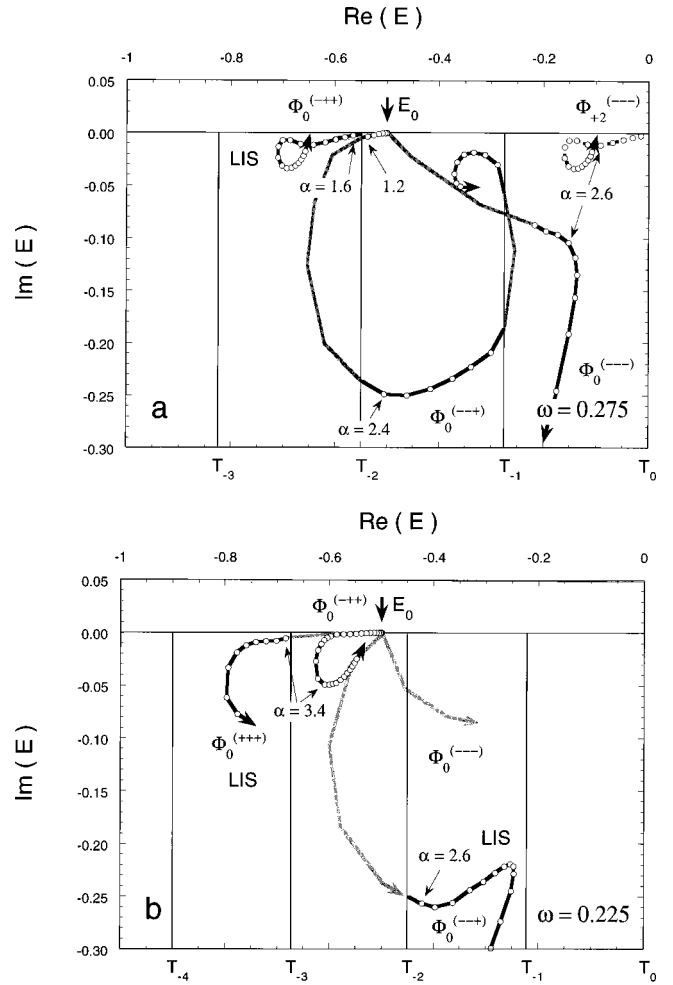FIG. 2. The same as Fig. 1. (a) $\omega = 0.35$, and (b) $\omega = 0.325$.

FIG. 3. The same as Fig. 1. (a) $\omega = 0.275$, and (b) $\omega = 0.225$.

For both the cases of $\omega = 0.55$ and 0.45, a pair of pole trajectories, $\Phi_0^{(---)}$ and $\Phi_0^{(-+)}$, has essentially the same shape. The pair, however, exchanges the role when ω is switched from $\hbar \omega < E_0$ to $\hbar \omega > E_0$. Namely, the branch $\Phi_0^{(---)}$ adiabatically correlates with the original bound state in the case of $\omega = 0.55$, but becomes the LIS in the case of $\omega = 0.45$.

At the onset of laser field $\alpha \sim 0$, the branch $\Phi_0^{(---)}$ runs left downwards, while the branch $\Phi_0^{(-+)}$ right downwards. Consequently, the resonance position of the original bound state exhibits a positive shift in the case of $\hbar \omega = 0.55 > E_0$, but a negative shift in the case of $\hbar \omega = 0.45 < E_0$. This is consistent with the fact that the sign of ac Stark shift changes at the one-photon ionization threshold $\hbar \omega = E_0$ [34].

In summary, a pair of pole trajectories sprouts from the pole of the original bound state on a different Riemann sheet. One of them corresponds to the adiabatic change of the original bound state, and the other is the origin of LIS's.

C. Encounter and switch of pole trajectories

In this section, we discuss the cases of lower laser frequency. We begin with the case of $\hbar \omega = 0.35$ shown in Fig. 2(a). Besides $\Phi_0^{(---)}$ and $\Phi_0^{(-+)}$, another pole $\Phi_0^{(-++)}$ is seen in the domain of $T_{-3} < \mathrm{Re}(E) < T_{-2}$. The latter is again

connected with the former pair at $E = -0.5$. In other words, three pole trajectories are grown from the original bound state at $E = -0.5$. These three poles are located on three different Riemann sheets, and two of them are shadow poles of the original bound state. As in the case of $\omega = 0.45$, it is $\Phi_0^{(--+)}$ that correlates with the original bound state. The resonance pole $\Phi_0^{(--+)}$ leaves the resonance sector when $\alpha = 3.2$, and becomes a ghost pole. It comes back to the resonance sector at $\alpha = 3.4$, and becomes a resonance again. This implies the death and resurrection of the resonance state. The other poles $\Phi_0^{(---)}$ and $\Phi_0^{(-++)}$ are LIS's.

Due to the translational symmetry with respect to $\mathrm{Re}(E)$, the LIS $\Phi_{+2}^{(---)}$, indicated by a dotted curve in the figure, has the same physical content as $\Phi_0^{(-++)}$ in the domain of $T_{-1} < \mathrm{Re}(E) < T_0$. The LIS's $\Phi_0^{(---)}$ and $\Phi_{+2}^{(---)}$ encounter with each other when α is at around 2.5. These two LIS's should be interacting with each other since these states have the same parity. This point will be discussed in Sec. IV by analyzing the wave functions of these resonance states.

In the case of slightly lower frequency $\hbar \omega = 0.325$ shown in Fig. 2(b), the topology of the encounter changes. The pair, $\Phi_{+2}^{(---)}$ and $\Phi_0^{(---)}$, seem to switch. It indicates that these two resonance states exchange their characters. Such an ex-

change is clearly reflected in the wave functions as discussed in Sec. IV.

When the frequency is set to a much lower value, the resonance sectors become much narrower. Figure 3(a) displays the case of $\hbar\omega = 0.275$. The pole $\Phi_0^{(--+)}$, which is grown from the original bound state, stays in the resonance sector only when $0 < \alpha < 1.4$, $2.4 < \alpha < 3.4$, and $3.6 < \alpha < 5.0$. Namely, the death and resurrection occur twice. Two LIS's, $\Phi_0^{(-++)}$ and $\Phi_0^{(---)}$, are seen. When one further lowers the laser frequency to $\hbar\omega = 0.225$, the trajectory correlating with the original bound state again shifts from $\Phi_0^{(--+)}$ to $\Phi_0^{(-++)}$ as can be seen in Fig. 3(b). This indicates that the shift in the role of the pole occurs at $\omega = E_0/2\hbar$ as well as at $\omega = E_0/\hbar$ [Figs. 1(a) and 1(b)]. We can infer that the shift occurs at every n-photon ionization threshold $\omega = E_0/n\hbar$ ($n = 1,2,3,...$).

The pole $\Phi_0^{(---)}$ does not enter any resonance sector in the case of $\hbar\omega = 0.225$. On the other hand, a newcomer, $\Phi_0^{(+++)}$, appears, and it behaves as a LIS. In this way, there are poles entering as well as leaving the resonance sector, and at least one LIS pole is always on the resonance sector even in the case of low frequency. This implies that the formation of LIS's is an ubiquitous phenomenon in intense laser fields.

D. Summary of the behavior of pole trajectories

The formation of LIS's has been predicted on the basis of the Kramers-Henneberger picture [23,24,26], which is valid only in the high-frequency fields. The present results show that the formation of LIS's occurs not only in the high-frequency domain, but also in the low-frequency domain, and is ubiquitous. It suggests that goodness of the Kramers-Henneberger picture is not required for the formation of LIS's.

The present results show that the LIS's originate from the shadow poles of the original bound state in the case of $\hbar\omega \leq E_0$. This is consistent with the results of Fearnside, Potvliege, and Shakeshaft in which LIS's originate from virtual states in the case of $\hbar\omega \sim 2E_0$, but from shadow poles of the original bound state in the case of $\hbar\omega \leq E_0$ [28].

Corresponding to the existence of the shadow pole on each Riemann sheet, branches of trajectory sprout from the original bound state. We hereafter call the branches altogether "pole-trajectory manifold." At every n-photon ionization threshold $\omega = E_0/n\hbar$, the branch adiabatically correlating with the original bound state is found to shift as $\Phi_0^{(---)} \rightarrow \Phi_0^{(--+)} \rightarrow \Phi_0^{(-++)} \rightarrow \cdots$. The other branches are the origins of LIS's.

In the case of small ω, the encounter and switch between pole trajectories occur frequently and in a complicated manner due to the small interval between adjacent Floquet blocks. Thus, resonance states would be subject to strong interaction and mixing.

Negative ions generally have a small number of bound states. The short-range potential model including ours is often regarded as mimicking negative ions [16]. Here, it is worthwhile to remark on neutral atoms. All neutral atoms

have an infinite number of bound states. We need to generalize the above findings to systems with a plural number of original bound states. In such a case, one has only to consider the pole-trajectory manifold for each original bound state and the interaction among manifolds. Since the direction of the resonance energy shift is generally opposite between the LIS and original state, one can distinguish the LIS from original states even when the number of original bound states is large. Difficulty in the generalization to realistic atoms would arise from many-electron character. In general, the importance of electron correlation is demoted by laser fields.

IV. CHARACTERS OF RESONANCE STATES

A. Kramers-Henneberger representation

In this section, we examine the resonance eigenvectors and discuss the physics underlying the phenomena described in the preceding section.

As will be seen, the eigenvectors in intense laser fields are very complicated superpositions of the null-field eigenstates, and it is difficult to base an interpretation on the character of wave functions. In such a case, the Kramers-Henneberger (KH) state in the acceleration gauge (the KH representation) is a useful alternative, particularly in the limit of high frequency [11,12].

In the acceleration gauge, the time-dependent Schrödinger equation is written as

$$i\frac{\partial}{\partial t}\Psi(p,t) = \frac{p^2}{2}\Psi(p,t) + \sum_{n=-\infty}^{\infty} e^{in\omega t} \int_{-\infty}^{+\infty} dp' U(p' - p) J_n[\alpha(p' - p)]\Psi(p',t), \quad (19)$$

where $J_n(p)$ is the nth order Bessel function. In the limit of high frequency, the Floquet-coupled equation in the acceleration gauge can be decoupled and reduced to the stationary Schrödinger equation with the Kramers-Henneberger Hamiltonian

$$H_{\mathrm{KH}} = H_0 = \frac{p^2}{2} + U_{\mathrm{KH}}, \quad (20)$$

where U_{KH} is the Kramers-Henneberger potential defined by

$$U_{\mathrm{KH}} = \int_{-\infty}^{+\infty} dp \int_{-\infty}^{+\infty} dp' |p\rangle U(p' - p) J_0[\alpha(p' - p)]\langle p'|. \quad (21)$$

The eigenstates of H_{KH} are called KH states. Although the KH states are exact eigenstates only in the limit of high frequency, they are expected to work as a good basis set in intense laser fields.

B. Assignment of resonance states in the KH representation

By expanding $\Phi_n(p)$ [see Eq. (6)] with KH states $\{\phi_i^{\mathrm{KH}}\}$, the Floquet eigenvector $\Phi(p,t)$ in the acceleration gauge can be expressed as follows:
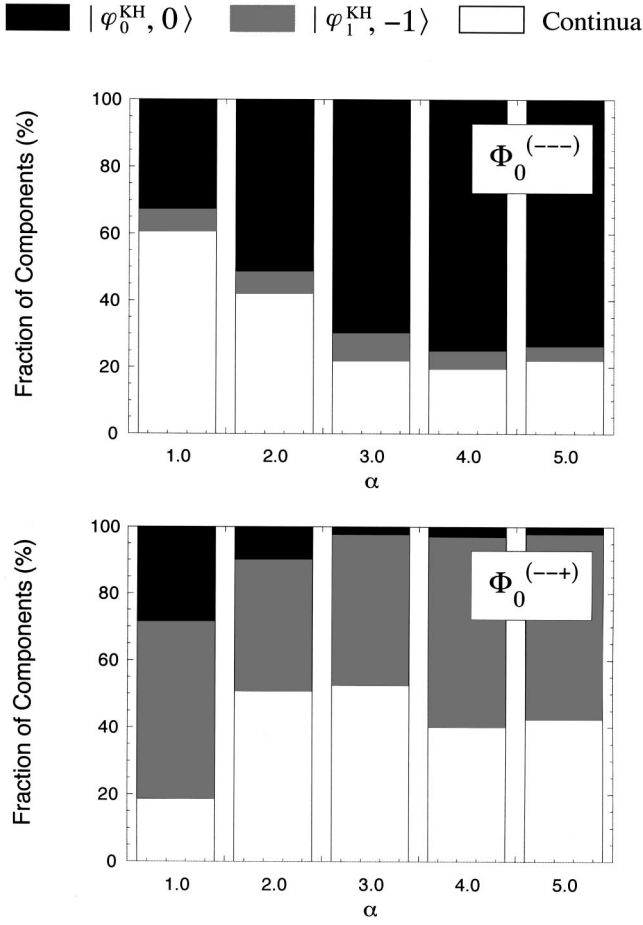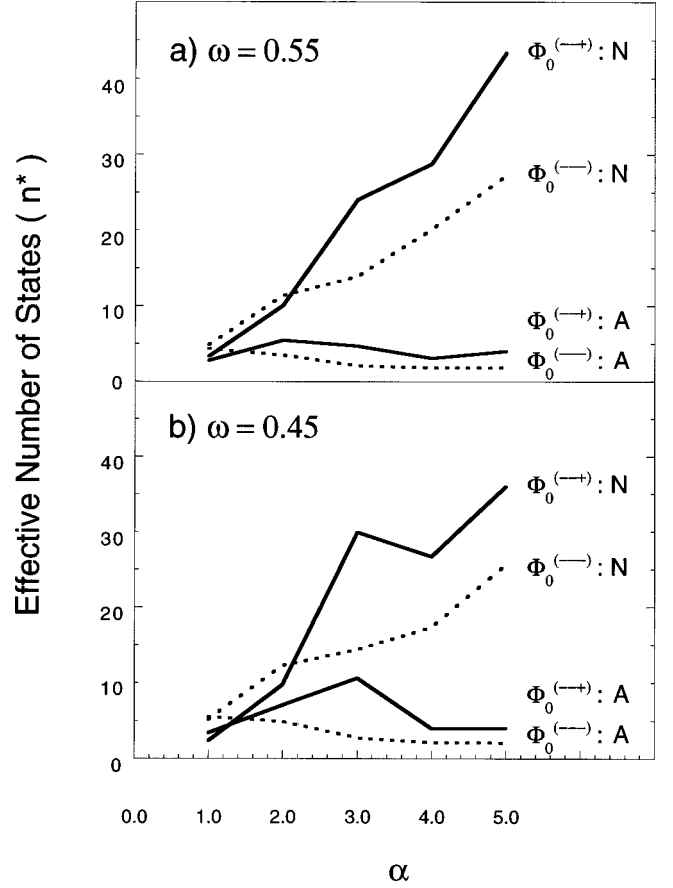
FIG. 4. The laser-intensity dependence of the fraction of the KH basis states in the resonance wave functions $\Phi_0^{(---)}$ and $\Phi_0^{(--+)}$.

$$\Phi(p,t) = \sum_{n=-\infty}^{\infty} \Phi_n(p)|n\rangle$$

$$= \sum_{n=-\infty}^{\infty} \sum_i |\Phi_i^{KH}\rangle\langle\phi_i^{KH}|\Phi_n\rangle|n\rangle$$

$$= \sum_{n=-\infty}^{\infty} \sum_i c_n^i |\Phi_i^{KH}\rangle|n\rangle$$

$$\equiv \sum_{n=-\infty}^{\infty} \sum_i c_n^i |\phi_i^{KH},n\rangle\!\rangle, \quad (22)$$

where $c_n^i \equiv \langle\phi_i^{KH}|\Phi_n\rangle$. Figure 4 shows the squared moduli of coefficient, $|c_n^i|^2$, for resonances $\Phi_0^{(---)}$ and $\Phi_0^{(--+)}$ in the case of $\omega=0.55$. Resonances $\Phi_0^{(---)}$ and $\Phi_0^{(--+)}$ are mainly composed of $|\phi_0^{KH},0\rangle\!\rangle$, $|\phi_1^{KH},-1\rangle\!\rangle$, respectively, and of continuum KH states. Here, we did not specify the contents of continua for the sake of simplicity. For different values of α ranging from 0.0 to 5.0, $|\phi_0^{KH},0\rangle\!\rangle$ and $|\phi_1^{KH},-1\rangle\!\rangle$ continue to be the main components of $\Phi_0^{(---)}$ and $\Phi_0^{(--+)}$, respectively. One can, thus, assign the resonances $\Phi_0^{(---)}$ and $\Phi_0^{(--+)}$ as $|\phi_0^{KH},0\rangle\!\rangle$ and $|\phi_1^{KH},-1\rangle\!\rangle$, respectively.

FIG. 5. The laser-intensity dependence of the effective number of states involved in the resonance wave functions $\Phi_0^{(---)}$ and $\Phi_0^{(--+)}$. Solid and dotted curves indicate $\Phi_0^{(--+)}$ and $\Phi_0^{(---)}$, respectively. The signatures A and N indicate the KH and null-field state representations, respectively. (a) The case of $\omega=0.55$, and (b) $\omega=0.45$.

On the other hand, the resonance wave functions in the normal gauge are complicated superpositions of various photon-number states and the spatial eigenstates of the null-field Hamiltonian. In order to discuss the complexity of resonance wave function in different representations, we analyze the effective number of states $n*$ given by Heller [35]:

$$n* = 1/\sum_{n,i} |c_n^i|^4. \quad (23)$$

Figure 5(a) shows the values of $n*$ for $\Phi_0^{(---)}$ and $\Phi_0^{(--+)}$ with changing laser intensity. The value of $n*$ is small and depends only weakly on the laser intensity in the KH representation, while it rapidly increases with the laser intensity in the null-field state representation. It is worth noting that the KH states work as a good basis even in the domain of such low frequency as $\omega=0.55$.

In the case of $\hbar\omega=0.45$ [Fig. 5(b)], the value of $n*$ is slightly larger than that in the case of $\hbar\omega=0.55$. However, the main component is still alive with dignity in the KH representation, and one can give the same assignment again for resonance poles, i.e., $\Phi_0^{(---)}$ and $\Phi_0^{(--+)}$ as $|\phi_0^{KH},0\rangle\!\rangle$

and $|\phi_1^{KH}, -1\rangle\rangle$, respectively. In short, both the resonances $\Phi_0^{(---)}$ and $\Phi_0^{(--+)}$ are interpretable as KH states.

C. Origin of the LIS from the point of view of KH states

As seen in Sec. III, $\Phi_0^{(--+)}$ and $\Phi_0^{(--+)}$ are LIS's for $\hbar\omega = 0.55$ and 0.45, respectively. According to the above discussion, these LIS's are assigned to $|\phi_1^{KH}, -1\rangle\rangle$ and $|\phi_0^{KH}, 0\rangle\rangle$, respectively. In the case of $\hbar\omega = 0.55$, the LIS $\Phi_0^{(--+)}$ is interpretable as a resonance resulting from a new KH bound state ϕ_1^{KH} formed by the deformation of the KH potential with increasing laser intensity.

In the case of $\hbar\omega = 0.45$, the LIS $\Phi_0^{(---)}$ has a character of the KH ground state ϕ_0^{KH} when $\alpha \geq 0.8$. The circumstance is not simple because ϕ_0^{KH} is not a newly formed state but a state that already exists in the limit of null field. It is caused by the shift of the branch expressing the LIS at one-photon threshold. In this case, the LIS formation is not explicable by the deformation of the KH potential, and should be considered as a shadow pole of the original bound state at most.

D. Mixing of resonance states at encounter and switch of pole trajectories

The encounter and switch of trajectories observed in Fig. 2 should be reflected in the component of resonance eigenvectors. In the case of $\hbar\omega = 0.35$ and 0.325 [Figs. 2(a) and 2(b)], resonance state $\Phi_0^{(---)}$ is approximately represented as $|\phi_0^{KH}, 0\rangle\rangle$ again. Figure 6(a) shows the change in the fraction of $|\phi_0^{KH}, 0\rangle\rangle$ contained in $\Phi_0^{(---)}$ and $\Phi_{+2}^{(---)}$ with changing laser intensity ($2.4 < \alpha < 2.8$) in the case of $\hbar\omega = 0.35$. One can see that the component in $\Phi_{+2}^{(---)}$ reaches the maximum exactly at the encounter of pole trajectories ($\alpha = 2.6$), while the component in $\Phi_0^{(---)}$ has the minimum at the same value of α. It indicates that resonances $\Phi_0^{(---)}$ and $\Phi_{+2}^{(---)}$ undergo mixing, which comes to the maximum when $\alpha = 2.6$. Figure 6(b) shows the case of $\hbar\omega = 0.325$. The figure demonstrates that resonance states $\Phi_0^{(---)}$ and $\Phi_{+2}^{(---)}$ exchange their characters with each other at $\alpha = 2.6$. Namely, the change in topology of pole trajectories observed in Fig. 2(b) is interpretable as a kind of avoided crossing between pole trajectories, and the exchange of the character of resonance states underlies it.

V. PHOTOELECTRON SPECTRA

Since the LIS is resonance state, it can be observed in photoelectron spectra. We calculate photoelectron spectra in intense laser fields, and discuss experimental detectability of the LIS. The photoelectron spectrum is expressed as the sum of transition probabilities from an initial state $|\phi_i\rangle\rangle$ to final Volkov states $|p', n\rangle\rangle$ with various momenta p' and photon numbers n:

$$P(E_f) \propto \sum_n \frac{1}{|p'|} |\langle\langle p', n|(\Omega^-(E_f))^\dagger|\phi_i\rangle\rangle|^2, \quad (24)$$
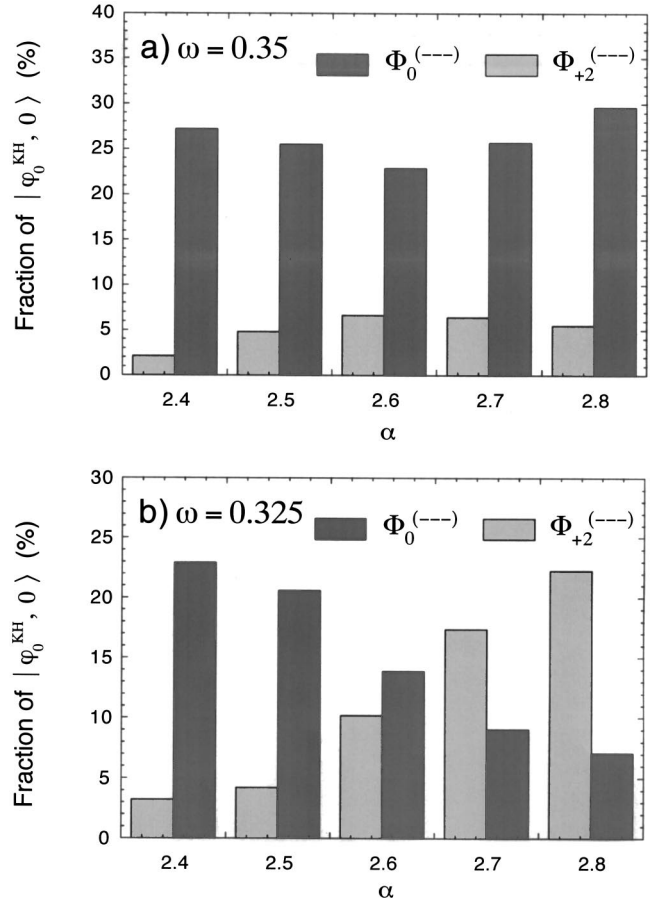
where

FIG. 6. The laser-intensity dependence of the fraction of $|\phi_0^{KH}, 0\rangle$ in the resonance wave functions $\Phi_0^{(---)}$ and $\Phi_{+2}^{(---)}$. (a) The case of $\omega = 0.35$ (encounter), and (b) $\omega = 0.325$ (switch).

$$E_f = \frac{p'^2}{2} + n\hbar\omega, \quad (25)$$

$\Omega^+(E)$ is the wave operator,

$$(\Omega^-(E_f))^\dagger = 1 + VG^\dagger(E_f), \quad (26)$$

and V is the interaction Hamiltonian with the complex scaling,

$$V = H_A - \frac{p^2}{2} = \sum_{l,m} \int\int dp''dp''' e^{-2i\theta}|p'', l\rangle\rangle$$

$$\times U[(p'''-p'')e^{-i\theta}]J_{l-m}[\alpha(p'''-p'')e^{-i\theta}]\langle\langle p''', m|. \quad (27)$$

By employing the acceleration gauge, the Volkov state $|p', n\rangle\rangle$ has a simple form,

$$|p', n\rangle\rangle = \delta(p - p') \otimes |n\rangle. \quad (28)$$

We consider the case of sudden excitation, and the initial state $|\phi_i\rangle\rangle$ can be written as

$$|\phi_i\rangle\rangle = \sum_j |\Phi_j\rangle\rangle\langle\langle\tilde\Phi_j|\phi_b, 0\rangle\rangle \equiv \sum_j |\Phi_j\rangle\rangle c_j, \quad (29)$$

where ϕ_b is the wave function of the bound state of the null-field Hamiltonian and $c_j \equiv \langle\!\langle \Phi_j | \phi_b, 0 \rangle\!\rangle$. The outgoing-boundary Green function $G^+(E_f)$ can be approximated by the spectral decomposition of the complex-scaled Floquet Hamiltonian [37]:

$$G^+(E_f) = \lim_{\epsilon \to +0} \frac{1}{E_f - H_F(p,t) + i\epsilon} \sim \sum_i \frac{|\Phi_i\rangle\!\rangle\langle\!\langle\Phi_i|}{E_f - E_i}. \tag{30}$$

By using the orthogonality of Floquet eigenvectors, one finally obtains

$$P(E_f) \propto \sum_n \frac{1}{|p|} \left| \sum_j c_j \left(\langle\!\langle p',n|\Phi_j\rangle\!\rangle + \frac{\langle\!\langle p',n|V|\Phi_j\rangle\!\rangle}{\frac{p'^2}{2} + n\hbar\omega - E_j} \right) \right|^2. \tag{31}$$

The explicit expressions for the matrix elements $\langle\!\langle p',n|\Phi_j\rangle\!\rangle$ and $\langle\!\langle p',n|V|\Phi_j\rangle\!\rangle$ are obtained by decomposing $|\Phi_j\rangle\!\rangle$ into the photon-number states $\Phi_j^n(p)$,

$$|\Phi_j\rangle\!\rangle = \sum_{n=-\infty}^{\infty} |n\rangle \Phi_j^n(p). \tag{32}$$

Using Eqs. (27), (28), and (32), one obtains the following expressions:

$$\langle\!\langle p',n|\Phi_j\rangle\!\rangle = \Phi_j^n(p') \tag{33}$$

and

$$\langle\!\langle p',n|V|\Phi_j\rangle\!\rangle = \sum_m \int dp'' e^{-2i\theta} U[(p''-p')e^{-i\theta}] J_{n-m}$$

$$\times [\alpha(p''-p')e^{-i\theta}] \Phi_j^m(p''). \tag{34}$$

Figure 7 shows the photoelectron spectra calculated using Eqs. (31), (33), and (34) for $\alpha = 1.0$ and three different frequencies, $\omega = 1.0$, 0.55, and 0.45. The spectra exhibit two progressions of peaks having the spacing of $\hbar\omega$. Each progression is ascribed to the above-threshold ionization. The number above each peak denotes the number of absorbed quanta $\hbar\omega$ before ionization. It should be noted that it is impossible to exactly determine the absorbed photon numbers because of following two reasons: (i) The photon number discussed here is defined in the acceleration gauge, and is different from that in the normal gauge; and (ii) the resonance states in intense laser fields are a superposition of various photon-number states.

In Fig. 7 one can see the peaks assigned to the LIS in all the spectra, and the contribution from the LIS appears most clearly in the case of $\hbar\omega = 0.55 \sim E_0$. This observation is interpreted by the following reasoning. Equation (31) indicates that the magnitude of contribution from the LIS is governed by the overlap integral, c_{LIS}, between the initial state $|\phi_b, 0\rangle\!\rangle$ and resonances $|\Phi_{LIS}\rangle\!\rangle$. In order to observe the LIS, one needs to choose a condition so as to give a large value of overlap. In high-frequency conditions such as $\omega = 1.0$, the origin of LIS's is not a shadow of the original bound state but a virtual state as was discussed by Fearnside, Potvliege,
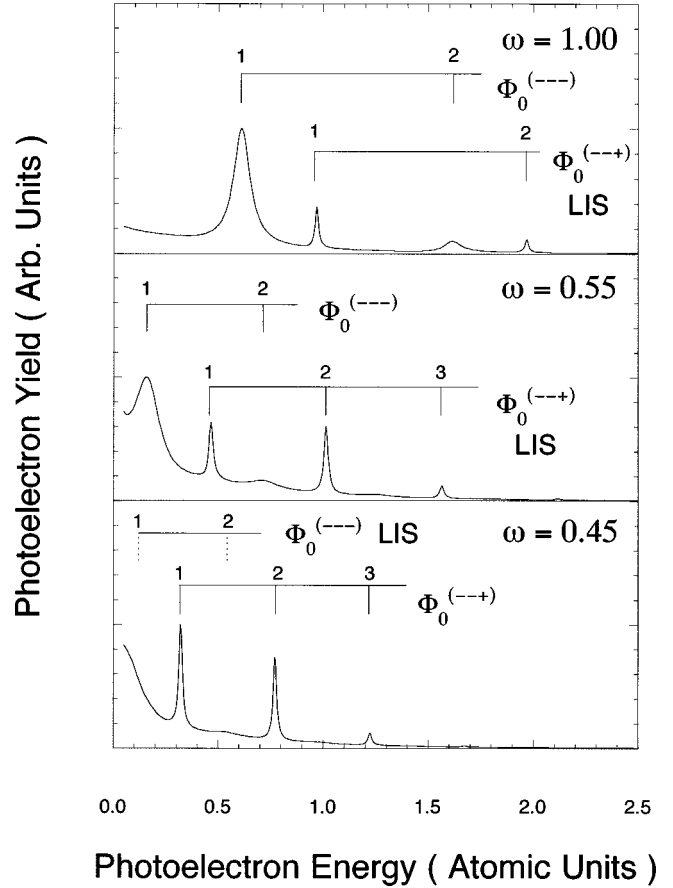

FIG. 7. Simulated photoelectron spectra for the cases with $\omega = 1.0$, 0.55, and 0.45.

and Shakeshaft [28]. The LIS's originating from a virtual state have no relation with the original bound state, and the overlap integral between them is expected to be small. On the other hand, under the condition of $\hbar\omega \sim E_0$, the LIS's originate from the shadow pole of the original bound state. In such a case, unless α is very large, the wave functions of LIS's should be similar to that of the original bound state, and the overlap integral should be large. The calculated values of $|c_{LIS}|$ are 0.3715, 0.7336, and 0.6945 in the case of $\alpha = 1.0$ and $\hbar\omega = 1.0$, 0.55, and 0.45, respectively. These values confirm the trend derived by the above argument. The small contribution of the LIS in the case of $\hbar\omega = 1.0$ results from the small value of overlap. On the other hand, the value of c_{LIS} in the case of $\hbar\omega = 0.45$ is comparable to that in the case of $\hbar\omega = 0.55$, but the contribution of the LIS in the case of $\hbar\omega = 0.45$ is also small. The following reason underlies it. The broad background signals in the region of low photoelectron energy are contribution from the direct ionization described by first term $\langle\!\langle p',n|\Phi_j\rangle\!\rangle$ in Eq. (31), and is found to be more intense in the lower frequency. In the case of $\hbar\omega = 0.45 < E_0$ [Fig. 7(c)], the background is more intense. Moreover, the LIS is switched from $\Phi_0^{(--+)}$ to $\Phi_0^{(---)}$, and the latter has a very large width. The interference between the background and broad resonance occurs, and the detection of the LIS peak becomes difficult. In conclusion,

the LIS is most clearly detectable if one uses the intense laser with the photon energy slightly larger than E_0.

VI. CONCLUSION

On the basis of the complex-scaled Floquet theory, we analyzed metastable states of model atom in intense laser fields. We concentrate on the condition for the formation of LIS's and its detectability. In the literature, the formation of LIS's has been discussed on the basis of the KH picture, which is valid only in the case of high frequency. However, the present study showed that LIS's exist even in the low-frequency intense fields, where the KH picture is not necessarily valid. The resonance wave functions are found to allow the assignment on the basis of KH states even in the case of $\hbar\omega < E_0$. However, the formation of LIS's is not explicable by the KH potential when $\hbar\omega < E_0$. This suggests that the formation of LIS's is independent of the goodness of the KH picture and ubiquitous for a wide range of laser frequency. From the behavior of pole trajectories on the complex energy plane, we found that the origins of LIS's are shadow poles of the original bound state when $\hbar\omega \lesssim E_0$. When the origin of the LIS is shadow pole and α is relatively small, the LIS gives rise to an intense peak in photoelectron spectra.

[1] *Atoms in Intense Laser Fields*, edited by M. Gavrila (Academic, New York, 1992).

[2] *Molecules in Intense Laser Fields*, edited by A. D. Bandrauk (Dekker, New York, 1994).

[3] A. Giusti-Suzor, F. H. Mies, L. F. DiMauro, E. Charron, and B. Yang, J. Phys. B **28**, 309 (1995).

[4] A. Hishikawa, S. Liu, A. Iwasaki, and K. Yamanouchi, J. Chem. Phys. **114**, 9856 (2001).

[5] J. H. Eberly, J. Javanainen, and K. Rzazewski, Phys. Rep. **204**, 331 (1991).

[6] L. V. Keldysh, Zh. Eksp. Teor. Fiz. **47**, 1945 (1964) [Sov. Phys. JETP **20**, 1307 (1965)].

[7] K. Coding and L. J. Frasinski, J. Phys. B **26**, 783 (1993).

[8] A. Hishikawa, A. Iwamae, and K. Yamanouchi, Phys. Rev. Lett. **83**, 1127 (1999).

[9] R. J. Levis, G. M. Menkir, and H. Rabitz, Science **292**, 709 (2001).

[10] H. Kono, S. Koseki, M. Shiota, and Y. Fujimura, J. Phys. Chem. A **105**, 5627 (2001).

[11] H. A. Kramers, *Collected Scientific Papers* (North-Holland, Amsterdam, 1956), p. 272.

[12] W. C. Henneberger, Phys. Rev. Lett. **21**, 838 (1968).

[13] M. Gavrila and J. Z. Kaminski, Phys. Rev. Lett. **52**, 613 (1984).

[14] M. Pont and M. Gavrila, Phys. Rev. Lett. **65**, 2362 (1990).

[15] J. H. Eberly and K. C. Kulander, Science **262**, 1229 (1993).

[16] G. Yao and S.-I. Chu, Phys. Rev. A **45**, 6735 (1992).

[17] M. Pont, N. R. Walet, M. Gavrila, and C. W. McCurdy, Phys. Rev. Lett. **61**, 939 (1988).

[18] M. Pont, N. R. Walet, and M. Gavrila, Phys. Rev. A **41**, 477 (1990).

[19] M. Gavrila and J. Shertzer, Phys. Rev. A **53**, 3431 (1996).

[20] N. A. Nguyen and T.-T. Nguyen-Dang, J. Chem. Phys. **112**, 1229 (2000).

[21] T. Zuo and A. D. Bandrauk, Phys. Rev. A **51**, R26 (1995).

[22] J. Shertzer, A. Chandler, and M. Gavrila, Phys. Rev. Lett. **73**, 2039 (1994).

[23] R. Bhatt, B. Piraux, and K. Burnett, Phys. Rev. A **37**, 98 (1988).

[24] J. N. Bardsley and M. J. Comella, Phys. Rev. A **39**, 2252 (1989).

[25] M. Dörr, R. M. Potvliege, D. Proulx, and R. Shakeshaft, Phys. Rev. A **43**, 3729 (1991).

[26] H. G. Muller and M. Gavrila, Phys. Rev. Lett. **71**, 1693 (1993).

[27] J. R. Taylor, *Scattering Theory* (Wiley, New York, 1972).

[28] A. S. Fearnside, R. M. Potvliege, and R. Shakeshaft, Phys. Rev. A **51**, 1471 (1995).

[29] J. H. Shirley, Phys. Rev. B **138**, B979 (1965).

[30] H. Sambe, Phys. Rev. A **7**, 2203 (1973).

[31] R. J. Eden and J. R. Taylor, Phys. Rev. B **133**, B1575 (1964).

[32] R. M. Potvliege and R. Shakeshaft, Phys. Rev. A **38**, 6190 (1988).

[33] W. P. Reinhardt, Annu. Rev. Phys. Chem. **33**, 223 (1982).

[34] N. L. Manakov, V. D. Ovsiannikov, and L. P. Rapoport, Phys. Rep. **141**, 319 (1986).

[35] E. J. Heller, Phys. Rev. A **35**, 1360 (1987).

[36] U. Peskin and N. Moiseyev, Phys. Rev. A **49**, 3712 (1994).

[37] B. R. Johnson and W. P. Reinhardt, Phys. Rev. A **28**, 1930 (1983).